Dispersion Effects on Membrane Reactor Performance

M. K. Koukou, N. Papayannakos, and N. C. Markatos
Dept. of Chemical Engineering, National Technical University of Athens, GR-157 80, Athens, Greece

A mathematical model has been developed that predicts the effects of design parameters, operating variables and physical properties on the performance of a membrane reactor with a permselective wall. The model consists of the full set of partial differential equations that describe the conservation of mass, momentum and chemical species, coupled with chemical kinetics and appropriate boundary conditions for the physical problem. The solution of this system is obtained by a finite-volume technique. The model was applied to study the dehydrogenation of cyclohexane. Two membrane types in tubular form were studied: a selective porous glass with low gas permeabilities and a porous alumina with very high gas permeabilities. It is concluded that gas separation and reactor performance are strongly influenced by dispersion effects only in the latter membrane reactor, while in both cases radial concentration profiles do not correspond to those obtained with plug flow. Therefore, simulations of this type of problem should be based on complex dispersion models rather than the existing ideal plug-flow ones.

Introduction

In modern technology membrane reactors are considered as an alternative to conventional reactors when separation during reaction enhances the reaction efficiency (Armor, 1989; Hsieh, 1991; Zaspalis and Burggraaf, 1991; Saracco and Specchia, 1994). These devices combine reaction and separation in a single unit, making the membrane reactor a cost-effective unit. They also make it possible to achieve significant enhancement over equilibrium conversion of feed composition, by continuous removal of the products during the reaction.

The last few years' research has been focused on the application of these reactors to increase conversions, especially of gas-phase equilibrium-limited catalytic reactions, to separate gases of industrial interest, to improve selectivity to intermediate products in consecutive catalytic reactions (Agarwalla and Lund, 1992), and so forth. New concepts and ideas have been investigated, so that membrane processes are today considered to be competitive with conventional gas-separation techniques. It is worthwhile noticing the use of membranes in the membrane reactor technology, which is extended to many traditional processes of commercial interest, such as dehydrogenations and partial dehydrogenations or oxidations (e.g., ammonia synthesis, water–gas shift reaction, oxidative coupling of methane, ethane dehydrogenation to ethylene) (Saracco and Specchia, 1994), steam reforming of natural gas (Uemiya et al., 1991), and dehydrogenation of propane to propylene. The most common configuration of a membrane reactor includes an annulus, the inner cylinder of which supports the membrane. The reacting fluid flows either inside or outside the inner tube while an inert gas flows either outside or inside the membrane tube, respectively. The membrane tube may be catalytically inert and enclose a conventional fixed bed of catalyst pellets (passive membrane system), or may be loaded with catalytic material (active membrane system) (Zaspalis, 1990). Inorganic-material-based membranes (ceramic or metallic, porous or dense) are particularly attractive for many high-temperature separations and for heterogeneous or homogeneous reactions, due to their inherent thermal, structural, and chemical stability.

In simulations of membrane reactors the assumption of plug-flow conditions for both fluids is generally considered (Becker et al., 1993; Itoh et al., 1988; Mohan and Govind, 1988; Okuba et al., 1991; Shinji et al., 1982; Tsotsis et al., 1992; Wu and Liu, 1992). In a recent study Itoh et al. (1994) have shown that for a membrane-separator system dispersion effects are significant. However, to the best of our knowledge, studies concerning the nonideal fluid-flow effects on reactor performance have not been reported in the literature.

The purpose of the present study is to investigate the influence of fluid dispersion on the performance of membrane reactors and to create a design tool for general application. Conversion and separation rates are compared with those calculated by the ideal plug-flow model, for typical reactors presented in the literature, for two types of membrane with different permeabilities (a porous glass membrane with low gas permeabilities and a porous alumina one with high gas permeabilities), and for two catalysts with different activities (Itoh et al., 1988; Okuba et al., 1991).

A rigorous two-dimensional mathematical model that simulates the flow field, taking into account radial and axial dispersion effects, and incorporating chemical reaction kinetics and membrane separation characteristics, is developed. This model and its solution algorithms are applied to study the performance of a typical membrane reactor with a permselective wall, and to compare conversions and separation rates with those calculated by the ideal plug-flow assumption for the model reaction of cyclohexane dehydrogenation.

Theoretical Analysis and Model Development

Physical problem considered

In the present work, the performance of an annular membrane reactor is studied. The feed gas passes through the catalyst bed, which is considered to be inside the inner tube of the annulus (feed side), as shown in Figure 1. The membrane, acting as a permselective barrier and allowing the selective passage of hydrogen from the reaction mixture across its structure, is considered to be on the inner cylinder surface. The reaction proceeds in the forward direction until equilibrium is reached. An inert gas (sweep gas) is fed into the space between the two tubes (separation side), sweeping the permeated gases to the outlet.

Mathematical problem

A two-dimensional, single-phase mathematical model for simulating the flow, chemical reaction, and separation through the membrane is developed. The following assumptions are made:

- Steady-state operation
- Isothermal ($T = 473$ K) operation at atmospheric pressure
- Cocurrent flow of sweep and feed gases.

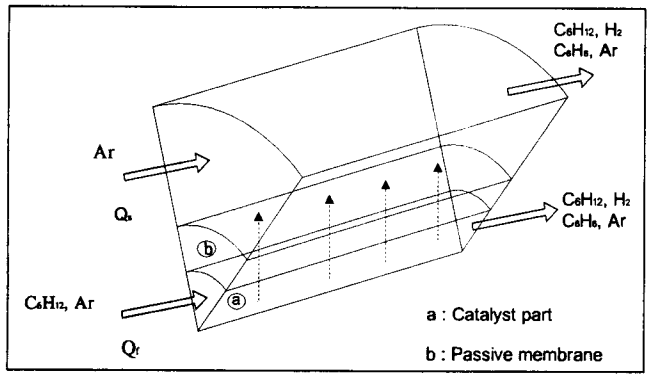

Figure 1. The system considered.

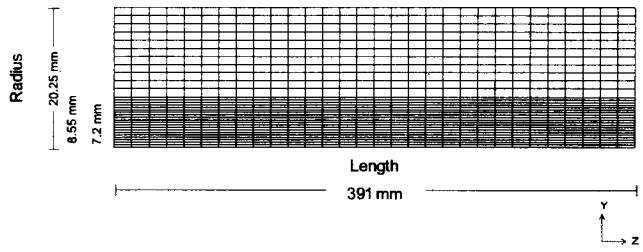

Figure 2. Typical grid used in the modeling (31 × 40).

It should be emphasized, however, that these assumptions do not present limitations of the model developed, which is general. They are useful simplifications that are dictated by the physical nature of the processes considered and make the discussion easier to understand.

Governing Partial Differential Equations. The mathematical analysis is based on the set of elliptic, partial differential equations that express the conservation of mass, momentum, and chemical species for steady, two-dimensional flow (Markatos and Moult, 1979; Spalding, 1981). As it is assumed that there is no angular variation of the dependent variables and there obviously exists flow symmetry, a polar-cylindrical (r, z) coordinate system is used, its two components r (radius), and z (length) being the independent variables of the problem (Figure 2).

The dependent variables are: pressure P (N/m^2), radial and axial velocity components v, w (m/s), and mass fractions of chemical species c_i (w/w).

The governing differential equations for all variables are expressed in the following general form (Markatos, 1989):

$$\frac{d}{dt}(\rho\phi) + \text{div}\{(\rho v\phi - \Gamma_\phi \,\text{grad}\,\phi)\} = S_\phi \qquad (1)$$

where

ϕ = dependent variable that, for the problem considered here, may be the two velocity components, v, w or the mass fractions c_i

ρ = density of the mixture

v = velocity vector

Γ_ϕ = appropriate effective exchange coefficient for variable ϕ, $\Gamma_\phi = \Gamma_{\phi l} + \Gamma_{\phi t}$, where $\Gamma_{\phi l}$ and $\Gamma_{\phi t}$ are laminar and turbulent contributions. In the momentum equations, Γ_ϕ is the transport coefficient that equals the mixture viscosity μ (Pa·s). In the mass-fraction equations Γ_ϕ are calculated as $\Gamma_\varphi = \rho D_i$, where D_i is a coefficient describing diffusive fluxes (in m^2·s^{-1})

S_ϕ = source-sink term per unit volume for variable ϕ, including both sources and sinks of variable ϕ (e.g., pressure gradient for the momentum equations), plus any other terms that cannot find a place on the lefthand side of the equation

When ϕ is equal to one, the mass-continuity equation is obtained. The first term on the lefthand side of Eq. 1 is, of course, zero for steady-state problems. More details may be found in the literature (Markatos, 1989).

Dispersion characteristics are taken from data presented by Carberry (Carberry, 1976). For the packed bed placed on the feed side of the reactor, radial and axial molecular diffusion are postulated for laminar flows (Bird et al., 1960). For higher flow rates in catalyst beds ($Re_p > 40$) the dispersion of the fluid can be estimated for values of Peclet number $Pe_r = 10$ and $Pe_z = 2$ ($Pe = Re \cdot Sc = d_p v/D$), which are independent of Re. On the separation side, molecular diffusivities are

used for laminar flow. For the turbulent flow region the radial Peclet number is equal to 10^3 and the axial one is equal to 10, while the dispersed plug-flow model was used (Carberry, 1976). Although the k-ϵ (or similar) model (Markatos, 1986) could have been used for the turbulent flow region, preliminary tests proved that the simplest (and most economical) model—that of using in the partial-differential equations specified enhanced transport coefficients (Γ_ϕ)—gave the same results, and it was thus preferred. Furthermore, this simple model is consistent with the way all the other coefficients are derived.

The solution of the preceding set of partial differential equations requires appropriate boundary conditions and special internal conditions (e.g., reaction rate, separation-rate equation) describing the physical problem considered. These conditions are presented in the following subsection.

The numerical problem

The set of the partial differential equations for the various ϕ's, along with the boundary and internal conditions is solved in an iterative manner (Spalding, 1980; Patankar and Spalding, 1972).

A grid, discretizing the space into a number of finite control volumes (cells), is used to cover the domain of interest. The conventional "staggered grid" arrangement is used (Patankar and Spalding, 1972), according to which the velocities are calculated at the middle of the computational cell faces to which they are normal, while the values of all other dependent variables are calculated at the center of the computational cells (Figure 3).

The differential equations are integrated over the control volumes, resulting in the corresponding set of finite-domain equations. The values of reactant and product concentration as well as the axial and radial velocities are calculated in each control volume. The radial velocities are practically zero compared to the mean axial velocity. The integration is similar neither to the Taylor series expansion, which is used by the classic finite-difference techniques, nor to the finite-element techniques, although it shares features of both, and it allows for direct physical interpretation of the mathematical manipulations.

The algorithm used to solve the preceding set of equations is the SIMPLEST algorithm embodied in the general PHOENICS package (Spalding, 1980, 1981; Markatos, 1989).

Application of the Model

Geometry — grid development

The detailed geometry of the membrane reactor, typical for laboratory use and performance tests of these systems (Becker et al., 1993; Itoh et al., 1988; Mohan and Govind, 1988; Okuba et al., 1991; Shinji et al., 1982) and the respective computational grid are illustrated in Figures 1 and 2. The reactor length is 391 mm, while the membrane thickness is 1.35 mm, the radius of the outer tube is 20.25 mm, and inner radius of the inner tube is 7.2 mm (Itoh et al., 1988).

A two-dimensional cylindrical polar grid was used that is uniform in the z direction and nonuniform in the r direction, and the choice of the grid size was dictated by grid independency studies, a pictorial summary of which is shown in Figures 4 and 5. In Figure 4, hydrogen partial-pressure axial profiles are shown for several grid sizes, in the z direction, for the case of the high-permeability membrane and plug-flow conditions. In Figure 5, hydrogen partial-pressure radial profiles are shown for several grid sizes in the r direction for the case with dispersion. It is observed that a 31×40 grid is the best choice for the plug-flow model, but it is more appropriate to use a 41×40 grid for the dispersion model. Similar runs were performed for the low-permeability membrane, and a 31×40 grid was found to be adequate for both models.

Boundary conditions

Inlet–Outlet. A mixture of cyclohexane and argon is fed at the inlet of the feed side. Argon is fed in a cocurrent manner on the separation side as a sweep gas, and it sweeps all the permeated gases to the outlet. Inlet feed rates are specified for all dependent variables and for both sides of the

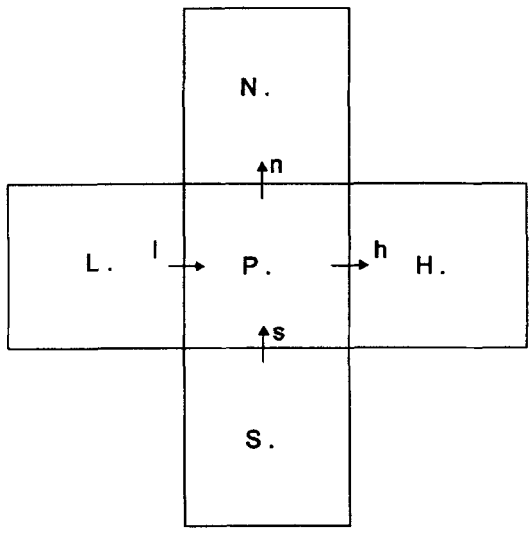

Figure 3. Staggered grid arrangement.
n,s,l,h: cell faces; *N, S, L, H, P*: cell centers.

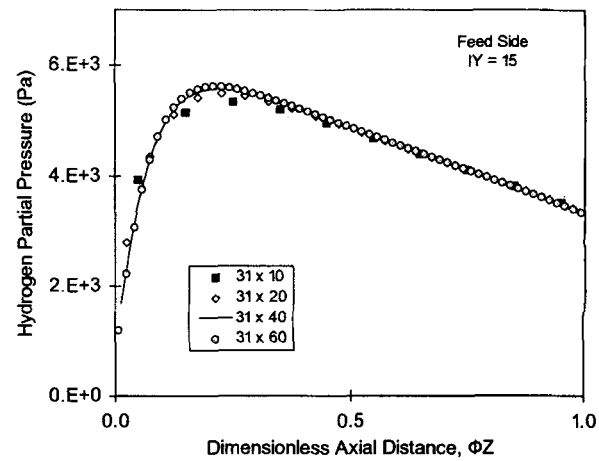

Figure 4. Hydrogen partial pressure axial profile on the feed side for various grids ($NY \times NZ$).
High-permeability membrane. Plug-flow conditions. Inlet feed rate = 0.5 kg/m^{2}s; inlet sweep-gas rate = 3.78 kg/m^{2}s.

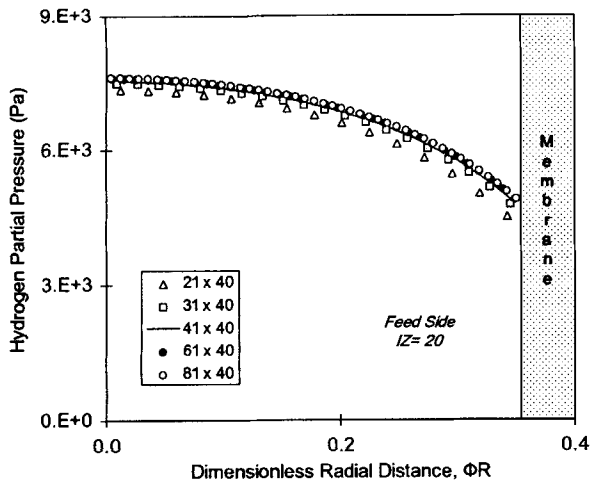

Figure 5. Hydrogen partial pressure radial profile on the feed side for various grids (NY × NZ).

High-permeability membrane. Dispersion case. Inlet feed rate = 0.5 kg/m^{2}s; inlet sweep-gas rate = 3.78 kg/m^{2}s.

computational domain (feed side, separation side). Typical ranges of the inlet fluxes (in kg/m^{2}s) and their compositions, are presented in Table 1. Uniform profiles were assumed for inlet species concentrations and for velocities.

At the outlet, the external pressure is considered uniform and equal to the atmospheric pressure, and therefore all computed pressures are relative to it. Because of the upwind interpolation (Spalding, 1980; Markatos, 1989), the profiles of all variables are properly calculated at the outlet.

Wall Friction. The no-slip condition is used for velocities, and the fluid-to-wall friction losses are computed by the log-law wall functions at all walls (Spalding, 1980).

Symmetry. Zero-flux conditions are applied at the symmetry plane for all variables.

Internal conditions and specific physical models

Separation-rate Equation. Two types of selective membrane in tubular form are studied. The first one is a microporous glass tube with a mean pore diameter of 4.0 nm and void fraction of 0.28. Permeability values of benzene, cyclohexane, hydrogen, and argon (calculated at $T = 473$ K) are taken from the literature (Itoh et al., 1988). The permeation of argon and hydrogen closely resembles Knudsen diffusion flow. The cyclohexane and benzene permeation flows deviate from Knudsen diffusion as temperature decreases due to surface diffusion. The second membrane is one with higher permeabilities corresponding to porous alumina (Okuba et al., 1991; Uhlhorn et al., 1989). Ceramic membranes are often used today, because of their good properties for separation and high thermal and chemical resistances. Permeability values used in the modeling for both membranes (high- and low-permeability membranes) are presented in Table 2.

Table 1. Typical Ranges of the Inlet Fluxes and Their Composition

		Inlet Flux mol/s	Composition w/w
Feed Side	LPM*	2.6E−6–8.5E−6	34% C_6H_{12}, 66% Ar
	HPM**	3.29E−4–9.87E−4	34% C_6H_{12}, 66% Ar
Separation Side	LPM	0.5E−4–4.E−4	100% Ar
	HPM	1.E−2–1.	100% Ar

*LPM: Low-permeability membrane.
**HPM: High-permeability membrane.

Table 2. Permeability Coefficients α_i (mol/m^2·s·Pa) Used in the Modeling

	LPM	HPM
α_{H_2}	2.95E−8	6.44E−6
$\alpha_{C_6H_{12}}$	6.43E−9	9.26E−7
$\alpha_{C_6H_6}$	9.51E−9	1.08E−6
α_{Ar}	7.23E−9	1.44E−6

The equation describing the permeation of species i through the membrane is (Itoh et al., 1988)

$$Q_i = \alpha_i(x_i P_f - y_i P_s), \tag{2}$$

where Q_i is the separation rate of component i (kg·m^{-2}·s^{-1}); α_i is the permeability coefficient of component i (kg·m^{-2}·s^{-1}·Pa^{-1}); x_i is the molar fraction of the component i on the feed side; y_i is the molar fraction of the component i on the separation side; P_f is the total pressure on the feed side (Pa); and P_s is the total pressure on the separation side (Pa).

Kinetic Expression. A literature survey was made in order to determine adequate kinetics expression for the cyclohexane dehydrogenation reaction over catalyst Pt/Al_2O_3 (Itoh et al., 1988; Okuba et al., 1991; Shinji et al., 1982). As a result, the following reaction-rate expression was used:

$$r = -\frac{k_C\left(k_P\frac{P_C}{P_H^3} - P_B\right)}{1 + K_B K_P \frac{P_C}{P_H^3}}, \tag{3}$$

$$k_c = A1\exp(-4{,}270/T) \qquad (\text{mol}\cdot\text{m}^{-3}\cdot\text{Pa}^{-1}\cdot\text{s}^{-1})$$

$$K_B = 2.03E-10\exp(6{,}270/T) \qquad (\text{Pa}^{-1})$$

$$K_P = 4.89E+35\exp(-26{,}490/T) \qquad (\text{Pa}^3)$$

where

$A1 = 0.221$ (mol·m^{-3}·Pa^{-1}·s^{-1})
P_i = partial pressure of component i

However, a wide range of catalyst activity was found (Itoh et al., 1988; Okuba et al., 1991). In the case of the low-permeability membrane, Eq. 3 was used (with $A1 = 0.221$) to describe the catalyst activity. In the case of the high-permeability membrane, as high fluxes can be attained, a kinetic expression is needed to describe a higher catalyst activity. For simplicity Eq. 3 is used again, but $A1$ was evaluated to equal 6.63 in order to describe the high catalyst activity as given by Okuba et al (Okuba et al., 1991).

Momemtum Loss in Packed Bed. The well-known Ergun equation was used to describe the momentum loss in the packed bed, in terms of pressure gradient (Bird et al., 1960):

$$\frac{\Delta_P}{L} = 150\frac{(1-\epsilon)^2\,\mu v_s}{\epsilon^3 d_p^2} + 1.75\frac{(1-\epsilon)v_s^2\rho}{\epsilon^3 d_p}, \tag{4}$$

where ΔP is the pressure drop (Pa); L is the length of the packed column (m); ϵ is the void fraction, equal to 0.38; μ is the laminar viscosity of the gaseous mixture; v_s is the superficial velocity ($m \cdot s^{-1}$), which is equal to $v_s = v_o \cdot \epsilon$, and v_o is the interstitial velocity in each control volume.

Cases studied

The following cases of membrane-reactor were studied:

1. A low-permeability membrane, corresponding to the microporous glass membrane, with a catalyst of moderate activity (Itoh et al., 1988).
2. A high-permeability membrane, corresponding to porous alumina with a high-activity catalyst (Okuba et al., 1991).

The results obtained from the model are compared to those predicted by the widely applied plug-flow model.

Computational details

Convergence was obtained readily by using relaxation of the false-time step type (Markatos, 1989) for the mass-fraction equations, and linear relaxation for the other variables. Runs were performed on a Silicon Graphics R4000 XS24 Indigo Workstation, and each iteration took about 1.5 s. A typical computer run, for the case with the high-permeability membrane using a grid of 31×40, required about 1,000 iterations to obtain full convergence for the plug-flow cases. For the dispersion cases many more iterations ($\sim 4{,}000$) were needed. Concerning the case with the low-permeability membrane and low reactor space-times, convergence was easily obtained after 2,000 iterations, but when higher space-times were used many more iterations were needed.

Results and Discussion

Verification of the model

The developed mathematical model has been verified against limited experimental data found in the literature (Itoh et al., 1988), for the case of the low-permeability membrane and assuming plug-flow conditions. As the predicted values compare well with the experimental values (Figure 6), it is concluded that the developed algorithm provides a realistic simulation of the membrane reactor performance.

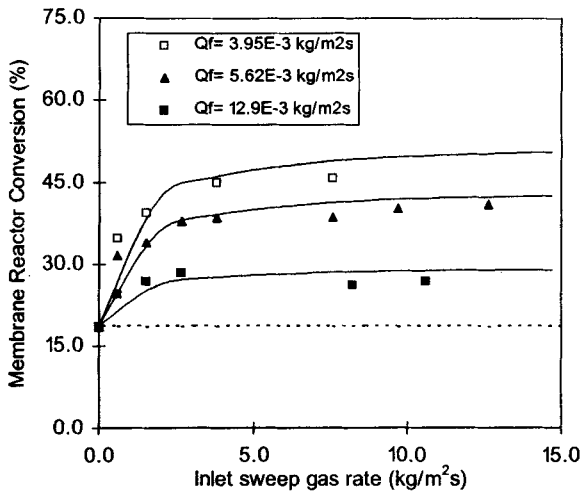

Figure 6. Model verification with experimental data from Itoh et al. (1988) (low-permeability membrane).

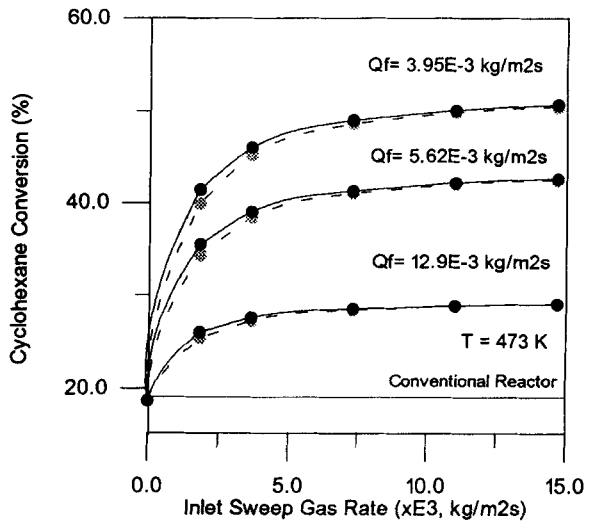

Figure 7. Cyclohexane conversion vs. Q_s (low-permeability membrane).

------ Plug-flow conditions; ---- dispersion conditions.

Cyclohexane conversions computed for the low-permeability membrane reactor are given in Figure 7. Although a conventional tubular reactor would reach equilibrium corresponding to the inlet gas composition with approximately a 19% cyclohexane conversion, the use of the membrane reactor strongly enhances conversions. The computed conversions for plug flow do not differ more than 1.5% from those computed by the dispersion model. This is also observed for the hydrogen recovery values in Figure 8. Therefore, cyclohexane conversion and hydrogen recovery values computed by the dispersion model and by the plug-flow model do not practically differ for high sweep-gas flow rates.

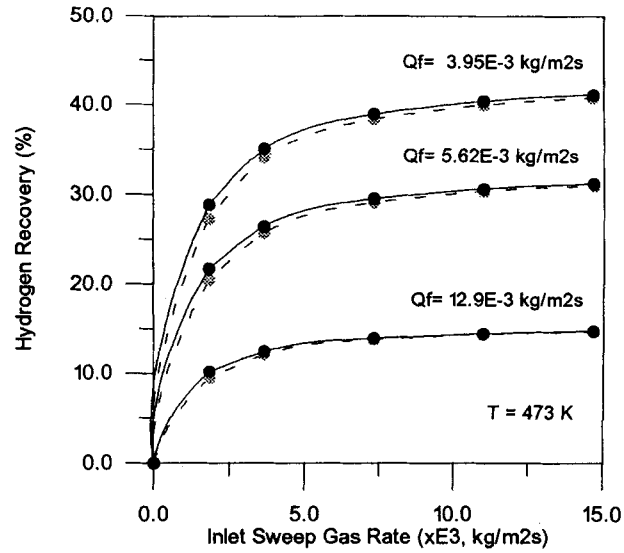

Figure 8. Hydrogen recovery vs. Q_s (low-permeability membrane).

------ Plug-flow conditions; ---- dispersion conditions.

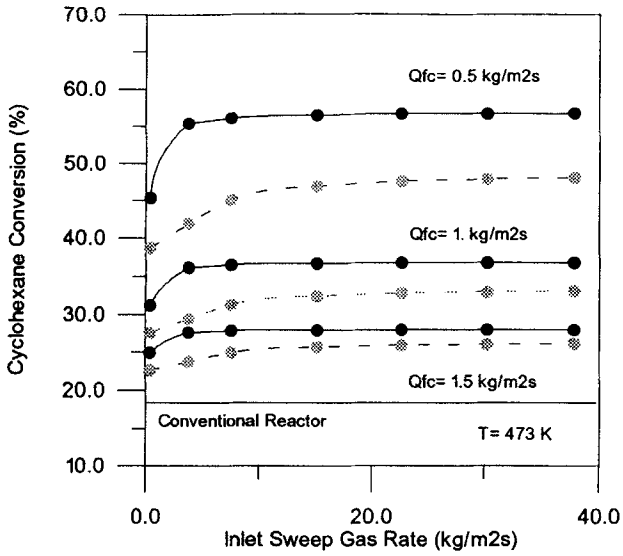

Figure 9. Cyclohexane conversion vs. Q_s (high-permeability membrane).

------ Plug-flow conditions; ---- dispersion conditions.

Cyclohexane conversions and hydrogen recoveries are given in Figures 9 and 10, respectively, for the high-permeability-membrane reactor. Unlike the low-permeability case, for which both models gave practically the same results, it is observed that considerable differences are computed when the dispersion model is adopted instead of the plug-flow one. In all cases examined, the dispersion model predicts lower values than those calculated by the plug-flow model, and the differences are in the range of 1.5–13.5% for the cyclohexane conversion and in the range of 2–16.5% for the hydrogen recovery. This behavior is explained by considering the increased radial fluxes in the case of the high-permeability membrane, in which the radial dispersion effects induce a stronger influence on the reactor performance.

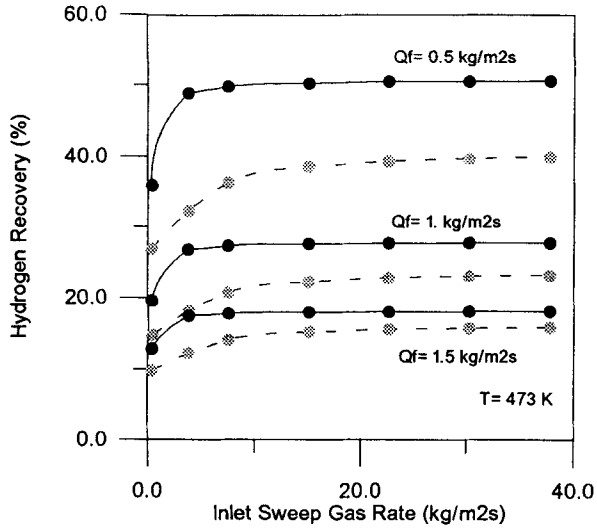

Figure 10. Hydrogen recovery vs. Q_s (high-permeability membrane).

------ Plug-flow conditions; ---- dispersion conditions.

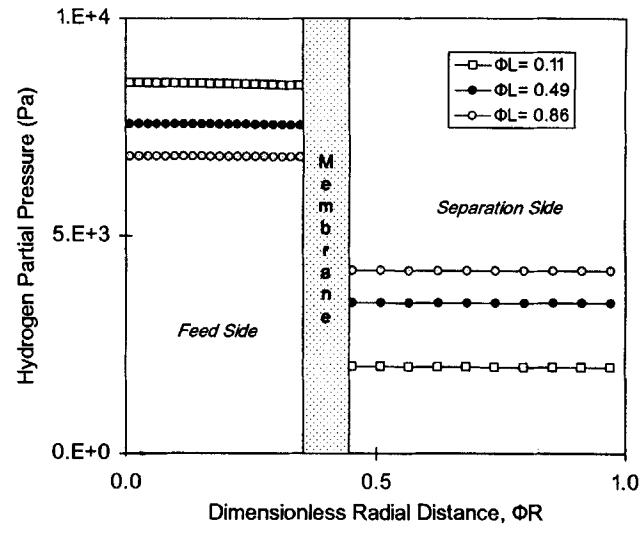

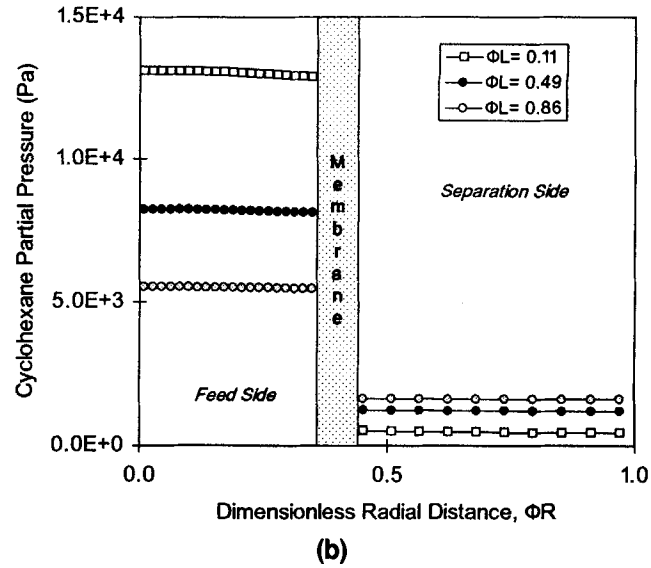

Figure 11. (a) Hydrogen partial pressure vs. radial distance; (b) cyclohexane partial pressure vs. radial distance.

Low-permeability membrane; inlet feed rate = 3.95E − 3 kg/m^2·s; Inlet sweep-gas rate = 1.85E − 3 kg/m^2·s.

The hydrogen partial-pressure profiles can give a better insight to the process. In Figure 11a and 11b radial hydrogen and cyclohexane partial-pressure profiles are given at three points along the membrane reactor length, for the low-permeability membrane. It is shown that on the feed side the profiles are rather flat, implying negligible influence of dispersion effects. On the separation side the partial-pressure profiles are flat as well. Thus, for the low-permeability membrane radial dispersion does not have an impact on the low radial fluxes, and the conversions computed by the plug-flow model and the dispersion model do not differ significantly, as discussed earlier.

On the contrary, for the high-permeability membrane the radial partial-pressure profiles are very different. In Figures 12a, 13a and 14a radial hydrogen partial-pressure profiles are

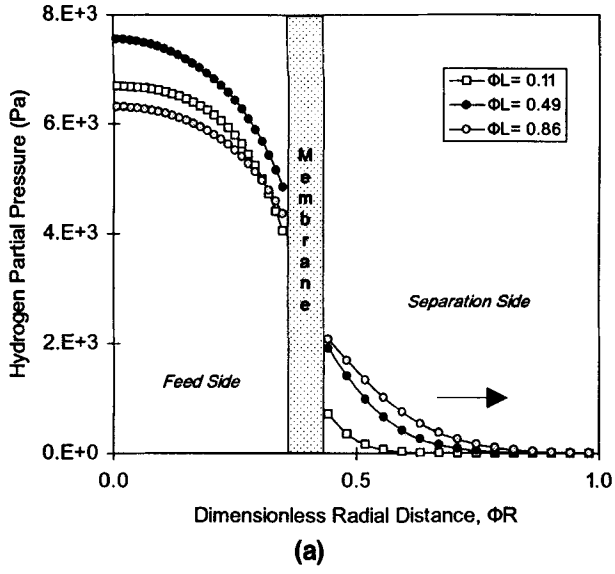

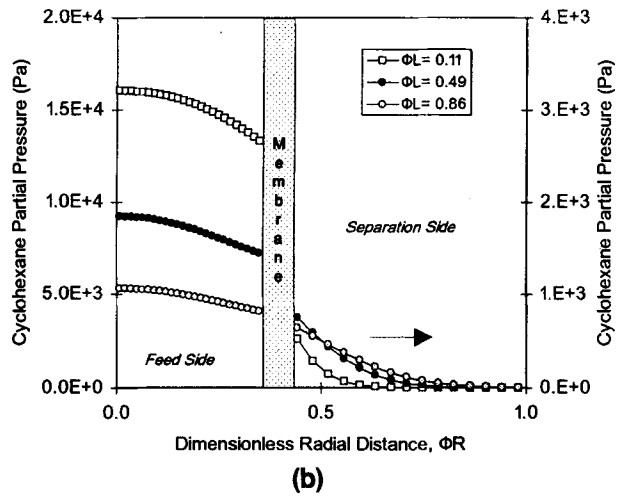

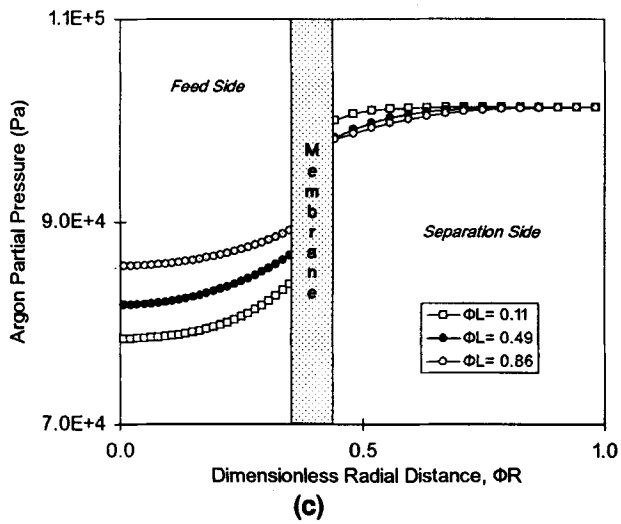

Figure 12. (a) Hydrogen partial pressure vs. radial distance; (b) cyclohexane partial pressure vs. radial distance; (c) argon partial pressure vs. radial distance.

High-permeability membrane; inlet feed rate = 0.5 kg/m^2·s; inlet sweep-gas rate = 3.78 kg/m^2·s.

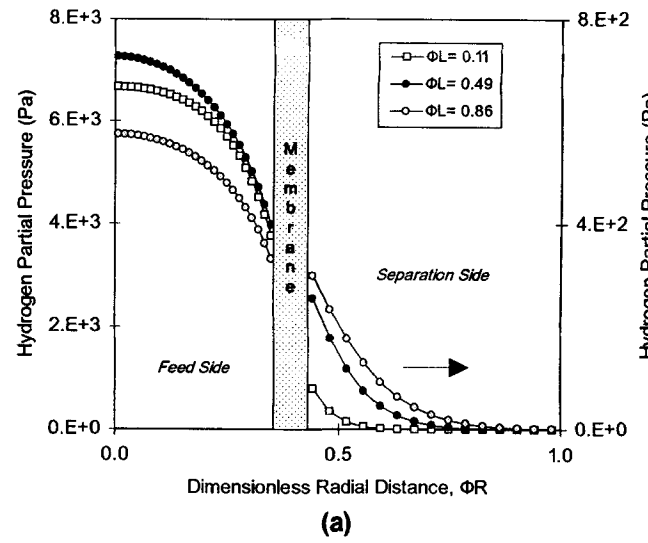

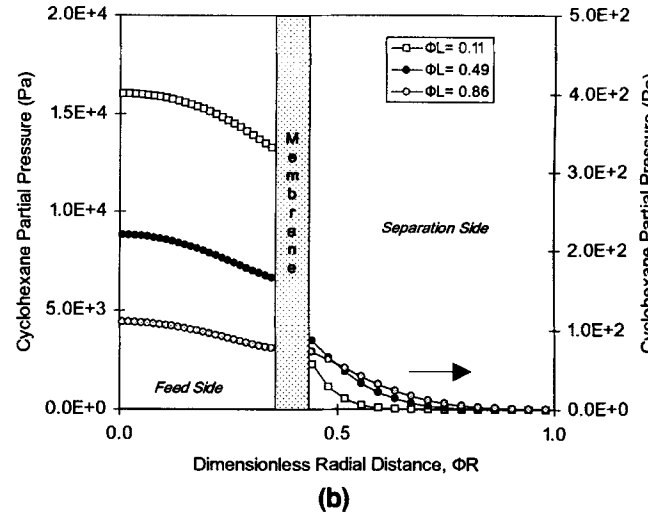

Figure 13. (a) Hydrogen partial pressure vs. radial distance; (b) cyclohexane partial pressure vs. radial distance.

High-permeability membrane; inlet feed rate = 0.5 kg/m^2·s; inlet sweep-gas rate = 30.25 kg/m^2·s.

drawn at three points along the membrane reactor length, for a wide range of inlet feed- and sweep-gas-rates. In all cases, it is shown that the profiles are not flat, implying that the partial-pressure difference, which is the driving force for the separation, decreases, which means that the influence of dispersion effects on both sides of the reactor is considerable. This phenomenon becomes more intensive when inlet feed rate decreases, causing a higher decrease in cyclohexane conversion and hydrogen recovery. As inlet feed rate increases, the gas velocity on the reaction side increases, the radial mass transfer increases, and the hydrogen removal rates are mainly controlled by diffusion inside the membrane and dispersion effects on the separation side. In Figure 12a, hydrogen partial pressure is shown to increase up to the middle of the reactor, and then to decrease up to the outlet of the reactor. This behavior is explained by considering that hydrogen diffuses through the membrane material to the separation side, but also that argon diffuses from the separation side to the

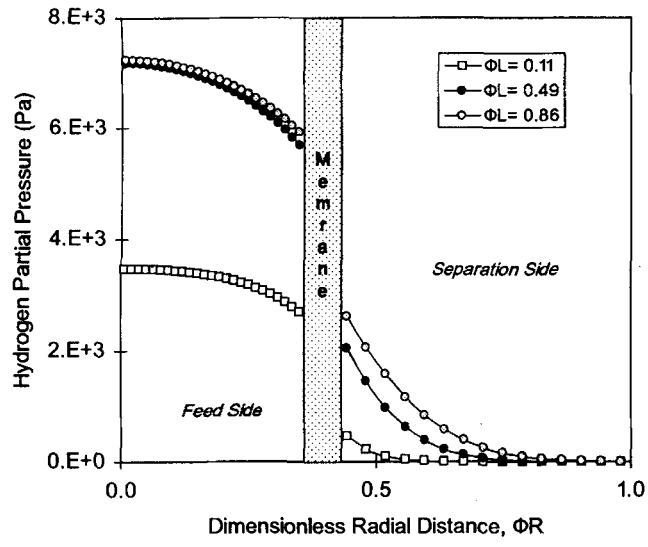

(a)

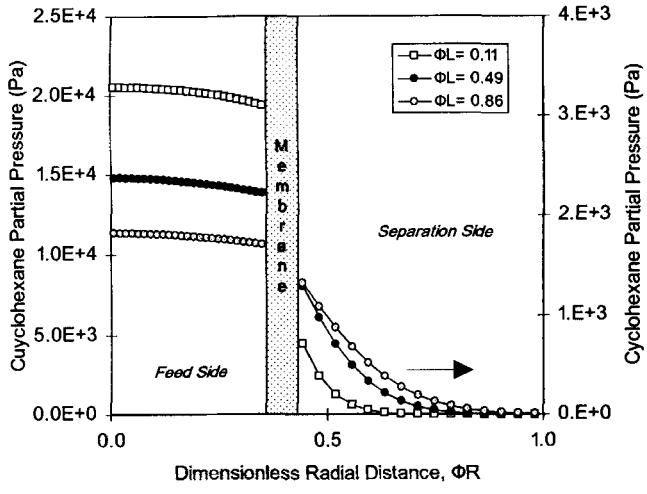

(b)

Figure 14. (a) Hydrogen partial pressure vs. radial distance; (b) cyclohexane partial pressure vs. radial distance.

High-permeability membrane; inlet feed rate = 1.5 kg/m^2·s; inlet sweep-gas rate = 3.78 kg/m^2·s.

feed side, diluting the reaction mixture and decreasing the partial pressure of hydrogen in it. Moreover, hydrogen production rates are high in the first part of the reactor, while in the second half they are reduced (Figure 12c).

The increase of the sweep-gas rate results in a decrease of hydrogen partial pressures on the separation side. Hydrogen removal rates become higher as hydrogen partial-pressure difference increases, and thus a higher decrease of the hydrogen partial pressure is noticed from the inlet to the outlet of the feed side, which induces a stronger influence of the dispersion effects on the hydrogen removal rates, as shown in Figures 12a and 13a.

In Figures 12b, 13b and 14b, cyclohexane partial-pressure radial profiles are presented. It is observed that these profiles suggest a strong influence of separation-side dispersion effects on cyclohexane removal from the reaction space. When the inlet feed rate decreases (Figure 12b), cyclohexane partial pressure on the feed side decreases and lower cyclohexane removal rates are observed, in comparison with those calculated by applying a higher inlet feed rate (Figure 14b).

Conclusions

In this study we develop a two-dimensional mathematical model, which simulates the flow field, chemical reaction, and separation through the membrane of a membrane reactor with a permselective wall. The model can predict the behavior of the membrane reactor under various operating conditions. Comparison of predictions with the limited experimental data found in the literature is very satisfying.

Cyclohexane dehydrogenation has been considered as a model reaction, for demonstration purposes and because of its important applications in practice. For a low-permeability membrane the use of the plug-flow model is proved to be a good simulation choice for the membrane reactor. As the permeabilities increase and the process becomes intensive, dispersion phenomena become important and simulation should be based on more complex dispersion models. Finally, dispersion effects on the separation side appear to be of equal importance to those on the feed side.

Acknowledgments

The authors express their thanks to CHAM Ltd., London, UK, for permitting the use of their product PHOENICS and to the European Union for partial funding of this research work.

Notation

d_e = equivalent diameter, m
d_p = particle diameter, m
D_r = radial diffusion coefficient, m^2·s^{-1}
D_z = aixal diffusion coefficient, m^2·s^{-1}
k_C = constant of rate equation, mol·m^{-3}·Pa^{-1}·s^{-1}
K_B = constant of rate equation, Pa^{-1}
K_P = constant of rate equation, Pa^3
l_o = reactor length, m
Q_f = inlet feed rate, kg/m^2·s
Q_s = inlet sweep gas rate, kg/m^2·s
r_{out} = outer radius of reactor, m
Re_p = ($= d_p u/h\upsilon$) particle Reynolds number
Re = ($= d_e u/h\upsilon$) Reynolds number
Sc = ($= \upsilon/D$) Schmidt number
$u_{C,i}$ = cyclohexane at feed side inlet, mol/s
$u_{C,o}$ = cyclohexane at feed side outlet, mol/s
$v_{C,o}$ = cyclohexane at separation side outlet, mol/s
$v_{H_2,o}$ = hydrogen at separation side outlet, mol H_2/s
X = membrane reactor conversion
ϵ = bed porosity
ν = kinematic viscosity, m^2/s
ϕZ = ($= l/l_o$), dimensionless reactor length
ϕR = ($= r/r_{out}$), dimensionless radius

Literature Cited

Agarwalla, S., and C. R. F. Lund, "Use of Membrane Reactor to Improve Selectivity to Intermediate Products in Consecutive Catalytic Reactions," *J. Memb. Sci.*, **70**, 129 (1992).

Armor, J. N., "Catalysis with Permselective Inorganic Membranes," *Appl. Catal.*, **49**, 1 (1989).

Becker, Y. L., A. G. Dixon, W. Moser, and Y. H. Ma, "Modelling of Ethylbenzene Dehydrogenation in a Catalytic Membrane Reactor," *J. Memb. Sci.*, **77**, 233 (1993).

Bird, R. B., W. E. Stewart, and E. N. Lightfoot, *Transport Phenomena*, Wiley, New York (1960).

Carberry, J. J., *Chemical and Catalytic Reaction Engineering*, McGraw-Hill, New York (1976).
Hsieh, H. P., "Inorganic Membrane Reactors," *Catal. Rev.-Sci. Eng.*, **33** (1,2), 1 (1991).
Itoh, N., Y. Shindo, K. Haraya, and T. Hakuta, "A Membrane Reactor using Microporous Glass for Shifting Equilibrium of Cyclohexane Dehydrogenation," *J. Chem. Eng. Japan*, **21**, 399 (1988).
Itoh, N., W. C. Xu, and K. Haraya, "Radial Mixing Diffusion of Hydrogen in a Packed-Bed Type of Palladium Membrane Reactor," *Ind. Eng. Chem. Res.*, **33**, 197 (1994).
Markatos, N. C., and A. Moult, "The Computation of Steady and Unsteady Turbulent, Chemically-Reacting Flows in Axisymmetrical Domains," *Trans. Instn. Chem. Eng.*, **57**, 156 (1979).
Markatos, N. C., "The Mathematical Modelling of Turbulent Flows," *Appl. Math. Modelling*, **10**, 190 (1986).
Markatos, N. C., "Computational Fluid Flow Capabilities and Software," *Ironmaking Steelmaking*, **16**, 266 (1989).
Mohan, K., and R. Govind, "Analysis of Equilibrium Shift in Isothermal Reactors with a Permselective Wall," *AIChE J.*, **34**, 1493 (1988).
Okuba, T., K. Haruta, K. Kusakabe, and S. Morooka, "Equilibrium Shift at Short Space-Time with Hollow Fiber Ceramic Membrane," *Ind. Eng. Chem. Res.*, **30**, 614 (1991).
Patankar, S. V., and D. B. Spalding, "A Calculation Procedure for Heat, Mass and Momentum Transfer in Parabolic Flows," *Int. J. Heat Mass Transfer*, **15**, 1787 (1972).
Saracco, G., and V. Specchia, "Catalytic Inorganic Membrane Reactors: Present Experience and Future Opportunities," *Catal. Rev.-Sci. Eng.*, **36**(2), 305 (1994).
Shinji, O., M. Misono, and Y. Yoneda, "The Dehydrogenation of Cyclohexane by the Use of a Porous Glass Reactor," *Bull. Chem. Soc. Japan*, **55**, 2760 (1982).
Spalding, D. B., "Mathematical Modelling of Fluid Mechanics, Heat Transfer and Chemical Reaction Processes; A Lecture Course," Rep. HTS/80/1, Imperial College, London (1980).
Spalding, D. B., "A General Purpose Computer Program for Multidimensional One or Two-Phase Flow," *Math. Comput. Simul.*, **13**, 267 (1981).
Tsotsis, T. T., A. M. Champagnie, S. P. Vasileiadis, Z. D. Ziaka, and R. G. Minet, "Packed Bed Catalytic Membrane Reactors," *Chem. Eng. Sci.*, **47**, 2903 (1992).
Uemiya, S., N. Sato, H. Ando, and E. Kikuchi, "Steam Reforming of Methane in a Hydrogen-Permeable Membrane Reactor," *Appl. Catal.*, **67**, 223 (1991).
Uhlhorn, R. J. R., M. H. B. J. Huis In't Veld, K. Keizer, and A. J. Burggraaf, "High Permselectivities of Microporous Silica-Modified γ-Aloumina Membranes," *J. Mat. Sci. Lett.*, **8**, 1135 (1989).
Wu, J. C. S., and P. K. T. Liu, "Mathematical Analysis on Catalytic Dehydrogenation of Ethylbenzene Using Ceramic Membranes," *Ind. Eng. Chem. Res.*, **31**, 322 (1992).
Zaspalis, V. T., "Catalytically Active Ceramic Membranes: Synthesis, Properties and Reactor Applications," PhD Thesis, Univ. of Twente, Enschede, The Netherlands (1990).
Zaspalis, V. T., and A. J. Burggraaf, "Inorganic Membrane Reactors to Enhance the Productivity of Chemical Processes," *Inorganic Membranes*, R. R. Bhave, ed., Van Nostrand Reinhold, New York (1991).

Manuscript received May 31, 1995, and revision received Jan. 11, 1996.